Ni *et al.*
Chinese Journal of Mechanical Engineering (2023) 36:75
https://doi.org/10.1186/s10033-023-00907-4

Chinese Journal of Mechanical Engineering

ORIGINAL ARTICLE

Open Access

Multi-physical Modeling and Adjusting for Ultrasonic Assisted Soft Abrasive Flow Processing

Yesha Ni[1,2], Yunfeng Tan[1,2] and Dapeng Tan[1,2*]

Abstract

The polishing efficiency of the soft abrasive flow (SAF) method is low, which is not in line with the concept of carbon emission reduction in industrial production. To address the above issue, a two-phase fluid multi-physics modeling method for ultrasonic-assisted SAF processing is proposed. The acoustics-fluid coupling mechanic model based on the realizable *k*-ε model and Helmholtz equation is built to analyze the cavitation effect. The results show that the proposed modeling and solution method oriented to ultrasonic-assisted SAF processing have better revealed the flow field evolution mechanism. The turbulence kinetic energy at different ultrasonic frequencies and amplitudes is studied. Simulation results show that the ultrasonic vibration can induce a cavitation effect in the constrained flow channel and promote the turbulence intensity and uniformity of the abrasive flow. A set of comparative polishing experiments with or without ultrasonic vibration are conducted to explore the performance of the proposed method. It can be found that the ultrasonic-assisted SAF method can improve the machining efficiency and uniformity, to achieve the purpose of carbon emission reduction. The relevant result can offer a helpful reference for the SAF method.

Keywords Soft abrasive flow, Ultrasonic vibration, Cavitation effect, Polishing efficiency, Turbulent kinetic energy

1 Introduction

Precision and ultra-precision mechanical parts play a significant role in the development of the aerospace industry, national defence industry, and microelectronics industry [1–3]. Finishing technology is a typical means to improve the surface quality of parts and reduce the surface roughness of work-piece [4, 5]. However, the traditional mechanical finishing method is not competent for some structured surfaces with small sizes and complex structures [6–8].

The soft abrasive flow (SAF) machining method [9] is a new method of abrasive flow finishing processing for various structured surfaces. The whole polishing process of the proposed method is as follows. The SAF characterized by low viscosity is firstly mixed in the tank, and then the abrasive flow is continuously pumped into the polishing tool. Due to the restriction of the constrained module, the abrasive flow enters into the constrained flow channel, where the flow velocity is up to the maximum, and the particle accumulation effect occurs. The work-piece surface located in the constrained flow channel is continuously impacted by the abrasive particles to achieve the surface polishing, as shown in Figure 1. However, the SAF processing method is inefficient and time-consuming, and the high-pressure pump used for fluid circulation has high power. Therefore, the whole system consumes enormous energy, which is not in line with the concept of carbon emission reduction in industrial production [10].

*Correspondence:
Dapeng Tan
tandapeng@zjut.edu.cn
[1] Key Lab of E & M, Ministry of Education and Zhejiang Province, Zhejiang University of Technology, Hangzhou 310014, China
[2] Collaborative Innovation Center of High-end Laser Manufacturing Equipment, Zhejiang Province & Ministry of Education, Hangzhou 310014, China

© The Author(s) 2023. **Open Access** This article is licensed under a Creative Commons Attribution 4.0 International License, which permits use, sharing, adaptation, distribution and reproduction in any medium or format, as long as you give appropriate credit to the original author(s) and the source, provide a link to the Creative Commons licence, and indicate if changes were made. The images or other third party material in this article are included in the article's Creative Commons licence, unless indicated otherwise in a credit line to the material. If material is not included in the article's Creative Commons licence and your intended use is not permitted by statutory regulation or exceeds the permitted use, you will need to obtain permission directly from the copyright holder. To view a copy of this licence, visit http://creativecommons.org/licenses/by/4.0/.

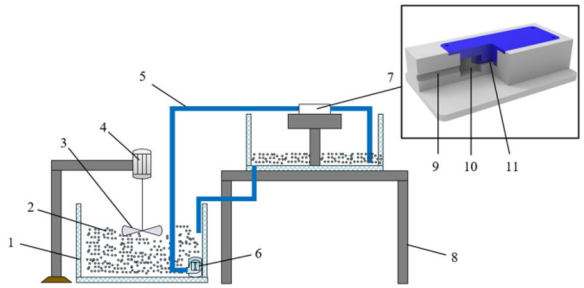

Figure 1 Schematic of soft abrasive flow processing: 1. Tank, 2. Soft abrasive flow, 3. Mixing blade, 4. Motor, 5. Outlet, 6. Pump, 7. Polishing tool, 8. Experiment table, 9. Circular entrance, 10. Turbulent region, 11. Constrained flow channel

To resolve the above matter, many research works have been performed. In 2011, Ji et al. proposed a design method for the sliding constraint module and verified the finishing efficiency through the experiment [11]. In 2012, Tan et al. researched the abrasive particle group distribution, dynamic characteristics, and near-wall micro-cutting mechanism in the constrained flow channel. They verified the feasibility and reliability of the SAF polishing method [12]. In 2012, Ji et al. presented a two-dimensional SAF dynamic model based on the topological structure transformation of the level set method (LSM). The model could describe the movement of the particles in turbulent flow and reveal the dynamical variation regulars of the phase surface of two-phase abrasive flow [13]. In 2016, Tan et al. redesigned the constrained flow passage using the fluid collision theory and presented a double-inlet SAF polishing method [14]. In their study, the fluid turbulent motion was described by the shear stress transport model, and the comparative polishing experiments proved that the double-inlet flow passage can increase the polishing efficiency. In 2018, Ji et al. established a gas-liquid-solid three-phase abrasive flow mechanics model based on the computational fluid dynamics-population balance model coupled method. They concluded that the effect of bubble collapse can effectively improve the processing efficiency and precision of the SAF method [15]. In 2018, Zhang et al. analyzed the processing mechanism on the curvature surface of the titanium alloy work-piece by the abrasive flow, and proposed a new material removal model of abrasive flow to reveal the processing regularities for complex geometric surfaces of titanium alloy artificial joints [16]. In 2018, Zhang et al. conducted a numerical simulation and experiment, and found that the lapping flow polishing efficiency and quality of complex titanium alloy surfaces could be improved by the triangular-constrained plates [17]. In 2020, Li et al. simulated the SAF field, and measured the SAF field by particle image velocimetry (PIV) to obtain its flow field characteristics [18]. In 2020, Li et al. proposed a calculation model to predict the motion locus of particles moving to a wall in boundary layers [19]. In 2021, Ge et al. proposed an ultrasonic assisted SAF method to resolve the low-polishing efficiency problem caused by the turbulent layer separation in SAF processing [20]. In 2021, Ge et al. adopted an innovative technique of a cavitation-based gas-liquid-solid abrasive flow polishing process to conclude that controlled polishing with cavitation erosion and abrasion can achieve a much higher quality surface on a large work-piece [21]. In 2021, Hu et al. analyzed the mechanism of the three-phase abrasive flow polishing method and built the three-phase abrasive flow model by the volume of fluid (VOF) method. It shows the jet effect produced by bubble collapse can effectively enhance the velocity and turbulent kinetic energy of local fluid [22]. In 2022, Zhou et al. built a basic SAF polishing mode with universal guiding significance and studied the effect of the spatial structure of constrained space on SAF polishing [23]. In 2023, Tan et al. established a mechanical dynamic model of the machining apparatus to obtain the flow field distribution of different structural parameters and developed an optimized processing apparatus to improve the machining efficiency [24].

From the above references, it can be inferred that current studies on the SAF method mainly focus on the facets of physical simulation and numerical modeling. The development degree of fluid turbulence is the main factor affecting the finishing effect of the SAF method [25]. However, the research on strengthening the turbulence intensity of solid-liquid two-phase flow is insufficient. Due to the structure of the constrained flow channel, the turbulence intensity in some local regions is inadequate, which leads to the dead angle of processing. In addition, there are some problems, such as long processing time, low efficiency, and high energy consumption. Therefore, it is necessary to research the dynamic characteristics of the SAF method, acquire the flow law of abrasive flow in the constrained flow channel, and improve the processing efficiency of the SAF method to achieve the purpose of carbon emission reduction. To resolve the above problems, a SAF polishing method using boundary ultrasonic vibration is presented in this paper [26]. As an acoustic emission technology, ultrasonic vibration can generate sound pressure and cavitation energy stably [27, 28]. The two-phase ultrasonic assisted SAF polishing process is a complex acoustics-fluid multi-physical issue with high nonlinear features, and the modeling-solving requires a large computation load [29]. The relevant difficult point is

the technological absence of a sound-fluid coupling modeling method for the SAF, which makes it challenging to reveal the ultrasonic assisted SAF processing mechanism.

In this paper, the leading scientific contribution is to propose a sound-fluid coupling modeling method oriented on the SAF, which can provide theoretical guides for researchers studying the ultrasonic assisted SAF processing mechanism. The multi-physical model, which includes a sound field and the flow field is built. Then, the calculation parameters are given, and the polishing process of the proposed method is analyzed by CFD-based calculation results. Finally, a polishing system is developed according to the processing principle of the proposed method, and the comparative polishing experiments are conducted to check the effectiveness of the proposed method.

2 Multi-physical Models

2.1 Fluid Control Equations and Multi-Phase Flow Model

The soft abrasive flow is a typical incompressible viscous fluid and keeps the continuity in the processing [30]. Therefore, it accords with the continuity equation and Navier-Stokes (N-S) equation [31, 32]

$$\frac{\partial \mu_i}{\partial x_i} = 0, \tag{1}$$

$$\rho\left(\mu_j \frac{\partial \mu_i}{\partial x_j} + \frac{\partial \mu_i}{\partial t}\right) = \rho K_i - \frac{\partial p}{\partial x_j} + \mu \frac{\partial^2 \mu_i}{\partial x_j \partial x_j} + \frac{\partial \tau}{\partial x_j}, \tag{2}$$

where μ_i, μ_j (i, j=1, 2, 3) represent the components of velocity vector μ in three coordinate directions; x_i, x_j represent the direction vector in three coordinate directions, p is the fluid pressure; ρ is the fluid density; μ is the kinetic viscosity; K_i is the gravity component; t is the time, and τ is the turbulent Reynolds stress:

$$\tau = -\rho\overline{u_i' u_j'} = \eta\left(\frac{\partial u_i}{\partial x_j} + \frac{\partial u_j}{\partial x_i}\right), \tag{3}$$

where μ_i', μ_j' are the fluctuation velocity values, and η is the turbulent viscosity.

Accordingly, by solving the continuity equation and N-S equation, the profiles of pressure and velocity in the constrained flow channel can be obtained [33, 34]. Moreover, the soft abrasive flow is a sparse two-phase flow [35]. In this hypothesis, the soft abrasive flow should have good fluidity and continuity.

It is assumed that the solid-phase abrasive particles are uniformly distributed in the liquid phase in the constrained flow channel [36]. The selection of a solid-liquid two-phase flow model mainly depends on the volume fraction of soft abrasive in solution. The abrasive fraction is less than 15%, and the equivalent diameter is small. As a multi-phase flow model, the Mixture model is suitable for simulating solid-liquid two-phase flow with sparse density [37]. Therefore, the Mixture model is used as the basic numerical model in this paper [38].

The Mixture model solves the momentum equation of the two-phase flow and describes the discrete phase through the relative velocity [39, 40]. The continuous equation of the mixed phase is

$$\frac{\partial}{\partial t}(\rho_m) + \nabla \cdot (\rho_m \boldsymbol{v}_m) = \dot{m}, \tag{4}$$

where ρ_m is the mixture density; $\boldsymbol{v}_m$ is the average velocity, and $\boldsymbol{m}$ is the mass transfer caused by the user-defined quality source or cavitation.

The momentum equation of the mixed phase is

$$\begin{aligned} &\frac{\partial}{\partial t}(\rho_m \boldsymbol{v}_m) + \nabla \cdot (\rho_m \boldsymbol{v}_m \boldsymbol{v}_m) \\ &= -\nabla p + \nabla \cdot \left[\mu_m\left(\nabla \boldsymbol{v}_m + \nabla \boldsymbol{v}_m^T\right)\right] + \rho_m \boldsymbol{g} \\ &+ \boldsymbol{F} + \nabla \cdot \left(\sum_{k=1}^{n} \partial_k \rho_k \boldsymbol{v}_{dr,k} \boldsymbol{v}_{dr,k}\right). \end{aligned} \tag{5}$$

2.2 Turbulence Model

Soft abrasive flow polishing is a complex nonlinear mechanic matter, and the disordered turbulent motion makes the work-piece surface obtain a relatively uniform surface texture. The soft abrasive flow field can be described by the turbulence models.

Under the larger time-averaged strain rate, the standard k-ε turbulence model might cause negative normal stress. Then, the normal stress item requires one or several mathematical constraints to make the turbulence computation accord with factual fluid motion regulars [41]. To resolve the above problem, the realizable k-ε model is proposed. It takes the empirical coefficient as a variable involving the turbulent kinetic viscosity and fluid strain rate, and contains a new pair of turbulence viscosity equation and dissipation rate equation [42, 43]:

$$\frac{\partial(\rho k)}{\partial t} + \frac{\partial(\rho k u_i)}{\partial x_i} = \frac{\partial}{\partial x_j}\left[\left(\mu + \frac{\mu_t}{\sigma_k}\right)\frac{\partial k}{\partial x_j}\right] + G_k - \rho\varepsilon, \tag{6}$$

$$\begin{aligned} &\frac{\partial(\rho\varepsilon)}{\partial t} + \frac{\partial(\rho\varepsilon u_i)}{\partial x_i} \\ &= \frac{\partial}{\partial x_j}\left[\left(\mu + \frac{\mu_t}{\sigma_\varepsilon}\right)\frac{\partial \varepsilon}{\partial x_j}\right] + C_1 E \rho\varepsilon - C_2 \rho \frac{\varepsilon^2}{k + (\nu\varepsilon)^{\frac{1}{2}}}, \end{aligned} \tag{7}$$

where k is the turbulent kinetic energy; μ_t is the turbulent viscosity coefficient; μ is the turbulent dissipation rate; σ_k, σ_ε are the Prandtl number of k and ε respectively; G_k is turbulent kinetic energy caused by average velocity gradient; E is the fluid strain; ν is the kinematic viscosity; C_1= 1.44, and C_2= 1.92.

For the standard k-ε model, the expression of the turbulent viscosity coefficient is

$$\mu_t = \rho C_\mu \frac{k^2}{\varepsilon}, \tag{8}$$

where C_μ is a constant. On the contrary, the realizable k-ε model takes C_μ as a variable:

$$C_\mu = \frac{1}{A_0 + A_s U^* k/\varepsilon}. \tag{9}$$

From the above equation, it can be inferred that it is a function of the time-averaged strain, coordinate rotating velocity, angular velocity, and turbulent parameters [44]. Therefore, the realizable k-ε model can accurately describe the inertial components of boundary layer fluid. Compared with the standard k-ε model and the renormalization group (RNG) k-ε model, it has the mathematical expression for Reynolds stress, which accords with the factual physical features of turbulent flow, adapting for multi-phase flow, shear flow, and jet flow. Based on the realizable k-ε model, the flow process of soft abrasive flow in the boundary layer near the work-piece surface can be described.

2.3 Acoustics Model

The equations used to describe the sound propagation in a fluid are derived from the governing equations for fluid flow. Most acoustic phenomena can be accurately described by classical pressure acoustics, in which flows are assumed to be lossless and adiabatic, viscous effects are ignored, and linear isentropic equations of state are used.

Based on the above assumptions, the sound field can be described as a variable, namely pressure p, which is controlled by the wave equation:

$$\frac{1}{\rho_0 c^2}\frac{\partial^2 p}{\partial t^2} + \nabla \cdot \left(-\frac{1}{\rho_0}\nabla p\right) = 0, \tag{10}$$

where t is the time, ρ_0 is the fluid density, and c is the sound velocity.

Acoustic problems often involve simple harmonics, such as sine waves. In general, any signal can be extended to harmonic components through its Fourier series. The wave equation can then be solved in the frequency domain for one frequency at a time. The form of harmonic solution is as

$$p(x,t) = p(x)e^{iwt}. \tag{11}$$

The actual (instantaneous) physical value of the pressure is the real part of the above equation. Based on this hypothetical pressure field, the transient wave equation can be reduced to the well-known Helmholtz equation:

$$\nabla \cdot \left(-\frac{1}{\rho_0}\nabla p\right) - \frac{\omega^2}{\rho_0 c^2} p = 0. \tag{12}$$

The periodic sound pressure fluctuation caused by ultrasonic vibration on the liquid phase can be described based on the above acoustic wave governing equation.

2.4 Cavitation Effect and Modification of Turbulence Model

Ultrasonic wave in the flow channel mainly produces the corresponding periodic pressure and the cavitation phenomenon [45, 46]. There is no perfect solution to the simulation of ultrasonic cavitation in the turbulent flow field. In this paper, the turbulence parameters are modified based on the existing turbulence model for the cavitation effect caused by ultrasonic vibration to carry out more accurate simulation research [47, 48]. The sound power of the sound field acts on the soft abrasive flow through sound pressure and its various effects. Sound power is the total energy radiated by a sound source per unit of time in space. In order to obtain the expression of sound power, it is necessary to derive the average sound energy density of the sound field. The energy provided by the sound vibration in the sound field is

$$E_k = \frac{1}{2}\rho_0 \mu^2 V, \tag{13}$$

where ρ_0 is the fluid density, and its corresponding potential energy is

$$E_p = -\int_0^p P\mathrm{d}V = \frac{V}{2\rho_0 c_0^2}\Delta p^2. \tag{14}$$

The energy density of sound is

$$\varepsilon = \frac{E_p + E_K}{V} = \frac{1}{2}\rho_0 \mu^2 + \frac{1}{2}\frac{\Delta p^2}{\rho_0 c_0^2}. \tag{15}$$

When the energy of the sound field is applied to the liquid phase, 4%–35% of the energy is transferred through the cavitation effect. Based on the realizable k-ε model, the transport equation of turbulent kinetic energy k is modified as

$$\frac{\partial(\rho k)}{\partial t}+\frac{\partial(\rho k u_i)}{\partial x_i} =\frac{\partial}{\partial x_j}\left[\left(\mu+\frac{\mu_t}{\sigma_k}\right)\frac{\partial k}{\partial x_j}\right]+G_k-\rho\varepsilon+S_k, \tag{16}$$

where S_k is the customized correction term of the model, which is based on the energy transfer generated by the cavitation effect, reflecting the influence of the cavitation effect on the flow field.

For the SAF method, polishing is achieved by the collision and friction of the abrasive particles on the work-piece surface. In particular, a large amount of turbulent kinetic energy is consumed by the friction collision between the particles and the work-piece surfaces after the ultrasonic vibration. However, the turbulence dissipation caused by friction is not reflected in the above transport equation of turbulent kinetic energy dissipation. Therefore, the turbulent kinetic energy dissipation equation of the realizable k-ε model is modified as

$$\frac{\partial(\rho\varepsilon)}{\partial t}+\frac{\partial(\rho\varepsilon u_i)}{\partial x_i} =\frac{\partial}{\partial x_j}\left[\left(\mu+\frac{\mu_t}{\sigma_\varepsilon}\right)\frac{\partial\varepsilon}{\partial x_j}\right] +C_1E\rho\varepsilon-C_2\rho\frac{\varepsilon^2}{k+(\nu\varepsilon)^{\frac{1}{2}}}+S_\varepsilon, \tag{17}$$

where $S\varepsilon$ is the modification of the dissipation equation.

The essence of turbulent dissipation of soft abrasive flow in near wall region is the energy conversion and transfer. The energy transformation is caused by the reaction force when the abrasive particles are micro-cutting the work-piece surface, and the reaction force can be regarded as the friction force of the soft abrasive flow. In addition, the SAF polishing is carried out by the shear stress of abrasive flow on the work-piece surface, so the friction force of fluid can also be expressed by the shear stress. The shear stress of the turbulent soft abrasive flow on the work-piece surface is composed of two parts, one is the viscous shear stress caused by the relative motion of the time-homogeneous flow layer, and the other one is the inertial shear stress caused by turbulence pulsation and momentum exchange between upper and lower layers of particles, its expression is

$$\tau=\tau_1+\tau_2=\mu\frac{\mathrm{d}u}{\mathrm{d}y}-\rho u^*v^*, \tag{18}$$

where μ is the fluid viscosity; u^* and v^* are the instantaneous fluctuating velocity.

To sum up, through the analysis of the turbulent state of the soft abrasive flow in the near wall region, the turbulence model is modified [49]. Hence, the effect of cavitation on turbulent kinetic energy and the friction caused by the shear force is introduced into the model [50]. Therefore, the modified realizable k-ε model can completely describe the turbulence dissipation in the SAF method.

3 Numerical Simulations

3.1 Numerical Model

The soft abrasive flow machining device is mainly composed of abrasive flow inlet, turbulence generating device, constrained flow channel, work-piece surface, and abrasive flow outlet, as shown in Figure 1(7). Among them, the constrained flow channel is the research object in this paper, as shown in Figure 1(11).

According to the above device, a 3D numerical model for the soft abrasive flow field is set up (shown in Figure 2). The numerical model adopts the free tetrahedral structure mesh and the total number of grid cells used for the flow passage is 130390. The physical conditions are as follows: the inlet of the flow channel is a circular passage with a diameter of 10 mm, and its boundary condition is the flow velocity inlet; the cylinder is a turbulence generator; the cuboid is the constrained flow channel, and it is 100 mm long, 10 mm wide, 5 mm high; the boundary condition of the outlet is the pressure outlet. The soft abrasive flow develops into turbulence in the turbulence generating device and enters the constrained flow channel to polish the work-piece surface. The ultrasonic vibration acts on the upper surface of the constrained flow channel, and its function is

$$W=A\sin\left(2\pi ft\right), \tag{19}$$

where A is the ultrasonic vibration amplitude, and f is the vibration ultrasonic frequency.

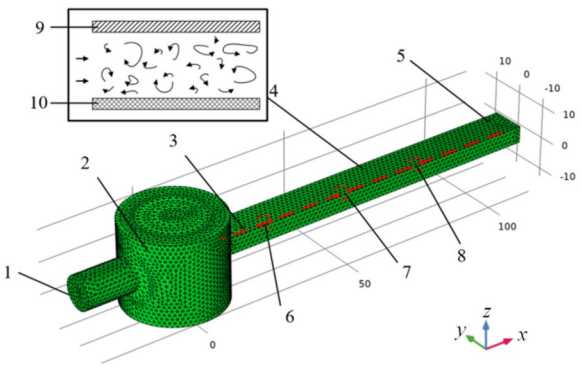

Figure 2 Numerical model for ultrasonic assisted soft abrasive flow processing: 1. Inlet, 2. Turbulence generator, 3. Detection line, 4. Constrained flow channel, 5. Outlet, 6. Monitoring point *a*, 7. Monitoring point *b*, 8. Monitoring point *c*, 9. Ultrasonic vibration, 10. Work-piece surface

Table 1 Physical parameters of soft abrasive flow

Parameters	Values
Particle-laden fluid	Water
Fluid viscosity (Pa·s)	0.001
Fluid density (kg/m^3)	998.2
Abrasive particle	Al_2O_3
Abrasive particle density (kg/m^3)	3500
Abrasive particle fraction	10%
Abrasive particle diameter (μm)	10

Table 2 Physical parameters of the flow field

Parameters	Values
Inlet velocity (m/s)	20
Outlet static pressure (Pa)	0
Boundary vibration amplitude (μm)	10, 20
Boundary vibration frequency (kHz)	0, 20 ,40

The lower surface of the constrained flow channel is the work-piece surface. The physical parameters of soft abrasive flow are listed in Table 1.

Due to the effect of ultrasonic vibration on SAF polishing, the flow field at the different frequencies and amplitudes were calculated respectively. The physical parameters of the flow field are shown in Table 2. The pressure discretization is interpolated by the standard algorithm. The scheme of the pressure-velocity coupling is the semi-implicit method for pressure-linked equations (SIMPLE), and the finite volume method is used to discretize the momentum, and turbulent kinetic energy according to the first-order upwind scheme [51, 52].

3.2 Cavitation Effect

After loading the ultrasonic vibration, the cavitation effect produced by ultrasonic in the liquid disturbs the distribution of velocity and turbulent kinetic energy intensity in the constrained flow channel, so as to strengthen the diffusion of each phase and promote the distribution of abrasive particles. Therefore, the characteristics of velocity distribution and turbulence intensity distribution in the constrained flow channel are the focus of this paper.

Since the velocity profile can reflect the flow field state of the polishing process, the velocity profiles near the work-piece surface of the steady state are acquired, as shown in Figure 3.

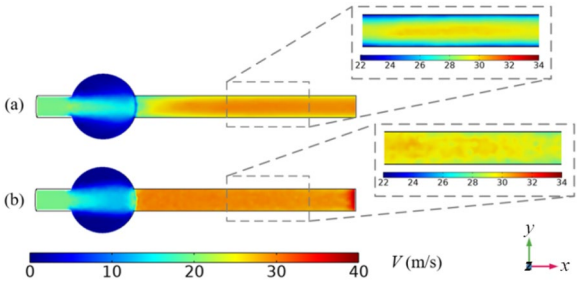

Figure 3 Velocity profiles of the constrained flow channel: (**a**) Stationary boundary, (**b**) A= 20 μm, f= 40 kHz

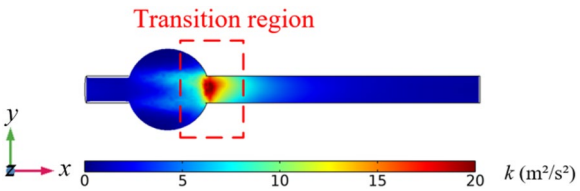

Figure 4 Turbulent kinetic energy profile of the constrained flow channel

In Figure 3, different colors represent different velocities of the abrasive flow. The flow rate of the left inlet is stable at 20 m/s, and the right constrained flow channel is the main research object of this paper. After loading ultrasonic vibration, the velocity in the constrained flow channel is enhanced and the distribution is more uniform. Especially at the edge of the work-piece surface, its uniformity is improved. In the region of ultrasonic vibration, local deceleration spots appear randomly in the flow field, as shown in Figure 3(b). The main reason for the deceleration spots is the ultrasonic cavitation effect caused by the loading ultrasonic vibration, which leads to the local high pressure and high temperature, and causes the stagnation of the flow field. From the perspective of velocity distribution, the ultrasonic vibration makes the whole work-piece surface more uniform, and it can improve the machining accuracy and efficiency of soft abrasive flow.

3.3 Effect of Ultrasonic Vibration on Turbulent Kinetic Energy

The turbulent kinetic energy is also a necessary physical parameter to characterize the turbulent performance of the constrained flow channel. Turbulent kinetic energy reflects the magnitude of turbulent pulsation energy. With the increase of turbulent kinetic energy, the abrasive particles collide more frequently with the work-piece surface, and the disordered motion of abrasive particles can improve the machining efficiency and precision.

Therefore, the turbulent kinetic energy profile of the stable state in the absence of ultrasonic action is acquired, as shown in Figure 4, and different colors represent different turbulent kinetic energy.

As the fluid flows from the turbulence generator to the constrained flow channel, the turbulent kinetic energy is reduced because of the molecular viscosity. The turbulent kinetic energy of the fluid near the wall decreases faster due to the viscous resistance of the wall. Apparently, the dissipation of turbulent kinetic energy not only reduces the efficiency of SAF polishing, but also affects the polishing uniformity.

In the transition region between the turbulence generator and the confined flow channel, the turbulent kinetic energy increases sharply due to the change of the flow channel size. However, the turbulent kinetic energy of the transition region is too strong to observe the distribution of the turbulent kinetic energy clearly in the constrained flow channel, and the transition region is not within the scope of processing. Hence, in order to facilitate the comparative analysis of the turbulent kinetic energy of the work-piece surface, the turbulent kinetic energy of the transition region should be filtered out. With respect to the issue, the turbulent kinetic energy profiles of the stable states with different ultrasonic frequencies are obtained, as shown in Figure 5, where the ultrasound amplitude is 20 μm.

It is easy to see that the turbulent kinetic energy in the core processing region is enhanced after loading the ultrasonic vibration. Accordingly, the higher ultrasonic frequency will cause a stronger turbulent kinetic energy, which proves that the turbulent kinetic energy dissipation can be alleviated by ultrasonic vibration. In Figure 5(b and c), owing to the higher ultrasonic frequency, the stronger turbulent kinetic energy is distributed in the core processing region, and forms a uniform processing surface. The above results show that the enhancement

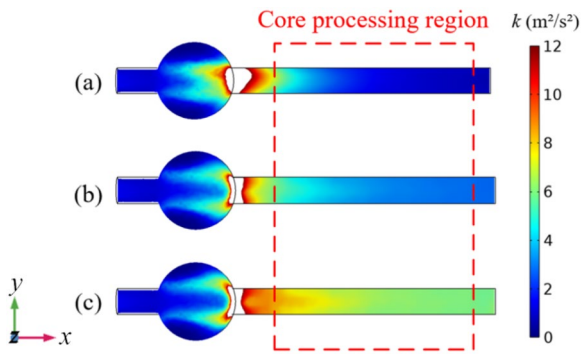

Figure 5 Turbulent kinetic energy profiles for different ultrasonic frequencies: (**a**) Stationary boundary, (**b**) $f = 20$ kHz; (**c**) $f = 40$ kHz

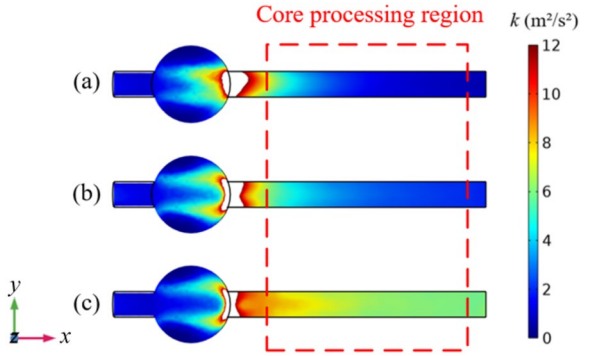

Figure 6 Turbulent kinetic energy profiles for different ultrasonic amplitudes: (**a**) Stationary boundary, (**b**) $A = 10$ μm, (**c**) $A = 20$ μm

of ultrasonic frequency not only improves the processing efficiency, but also markedly improves the polishing uniformity.

In order to study the effect of the ultrasonic amplitude on the SAF polishing, the turbulent kinetic energy profiles of the stable states with different ultrasonic amplitudes are obtained, as shown in Figure 6, where the ultrasound frequency is 40 kHz. In Figure 6, the increase of the ultrasonic vibration amplitude can improve the turbulent kinetic energy near the work-piece, which indicates that the high vibration amplitude is beneficial to the increase of the particle-wall impacting frequency.

As for a further study on the relationship between ultrasonic vibration and flow field, the three monitoring points near the work-piece surface are selected, as shown in Figure 2(6–8). Subsequently, the turbulent kinetic energy time-varied waves of the three monitoring points are obtained, as shown in Figure 7, where the legend represents the x coordinate of each point, and the ultrasound amplitude is 20 μm. From the figure, it can be inferred that the turbulent kinetic energy of each monitoring point is affected by the ultrasonic vibration, and its turbulent kinetic energy intensity is positively correlated with the ultrasonic frequency. Moreover, each monitoring point has a smooth transition region in which the turbulent kinetic energy reaches a stable value and does not change with time. The smooth transition region divides the entire curve into two parts, the front part is called region A, and the back part is called region B. The increase of turbulent kinetic energy in region A is mainly caused by the ultrasonic vibration of the flow channel. Then in the smooth transition region, the turbulent kinetic energy dissipation in the constrained flow channel is consistent with the turbulent kinetic energy generated by the ultrasonic vibration. After the smooth transition region, the soft abrasive flow passes through the turbulence generator into the constrained flow channel. At this

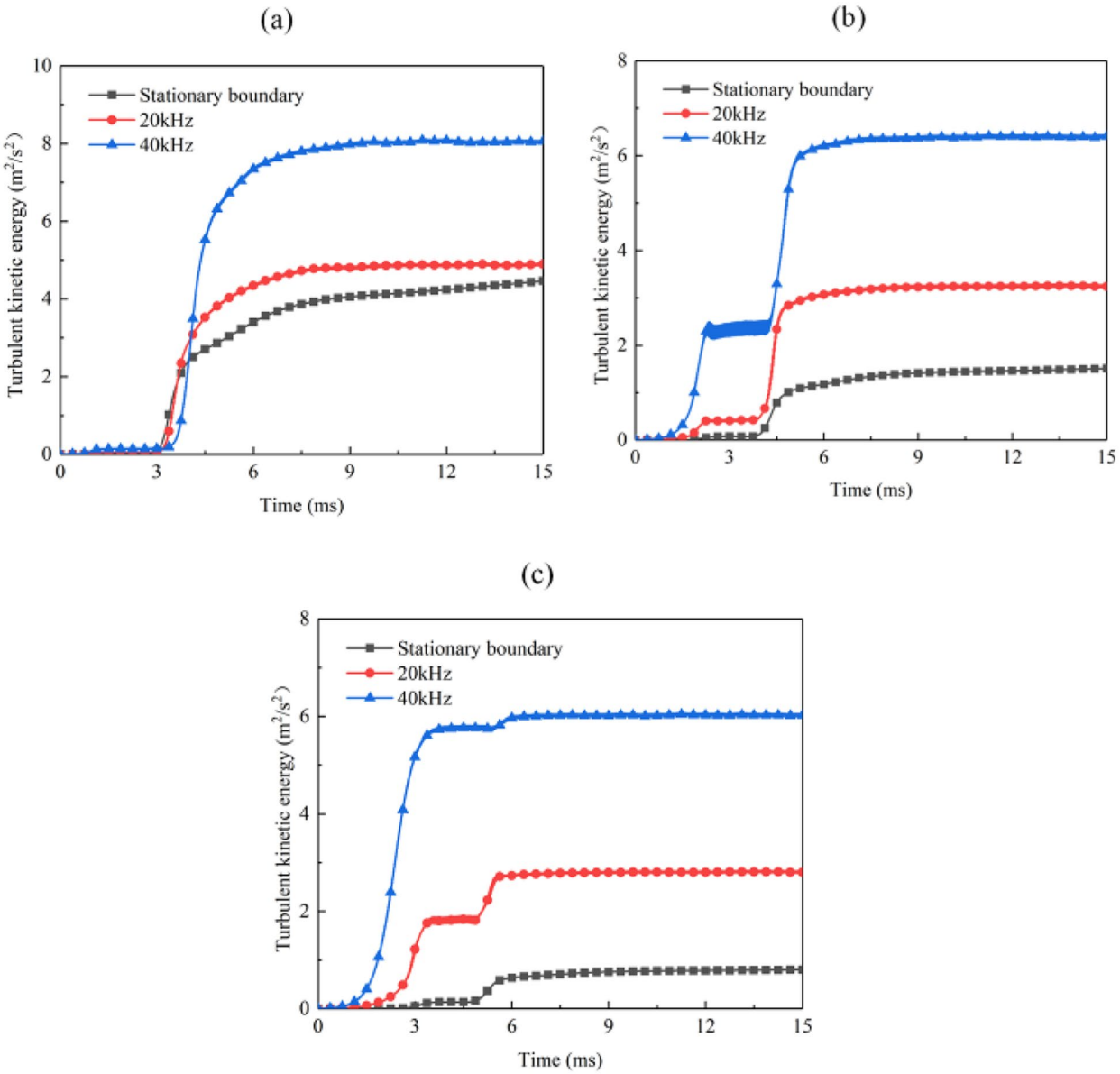

Figure 7 Turbulent kinetic energy time-varied waves for different monitoring points: (**a**) $x = 40$ mm, (**b**) $x = 70$ mm, (**c**) $x = 100$ mm

point, under the combined action of the ultrasonic vibration and the turbulent abrasive flow, the turbulent kinetic energy of the flow field continues to rise and finally reaches a stable state.

By comparing the three monitoring points, it is easy to see that the turbulent kinetic energy of point *a* almost remains unchanged in region A, while the turbulent kinetic energy of point *c* increases most rapidly. Apparently, the turbulent kinetic energy increases faster with the increase of ultrasonic frequency. The above results show that the turbulent kinetic energy of each point in region A is related to its location, and the effect of ultrasonic vibration is more pronounced when the monitoring point is farther away from the turbulence generator.

However, the variation of the turbulent kinetic energy of each point in region B is opposite to that in region A, and the turbulent kinetic energy of point *a* rises rapidly in region B with the most significant increase in amplitude. The increase of turbulent kinetic energy in region B is mainly caused by the abrasive flow from the turbulence generator. The above results show that the turbulent kinetic energy of each point in region B is also related to its location, and the effect of the abrasive

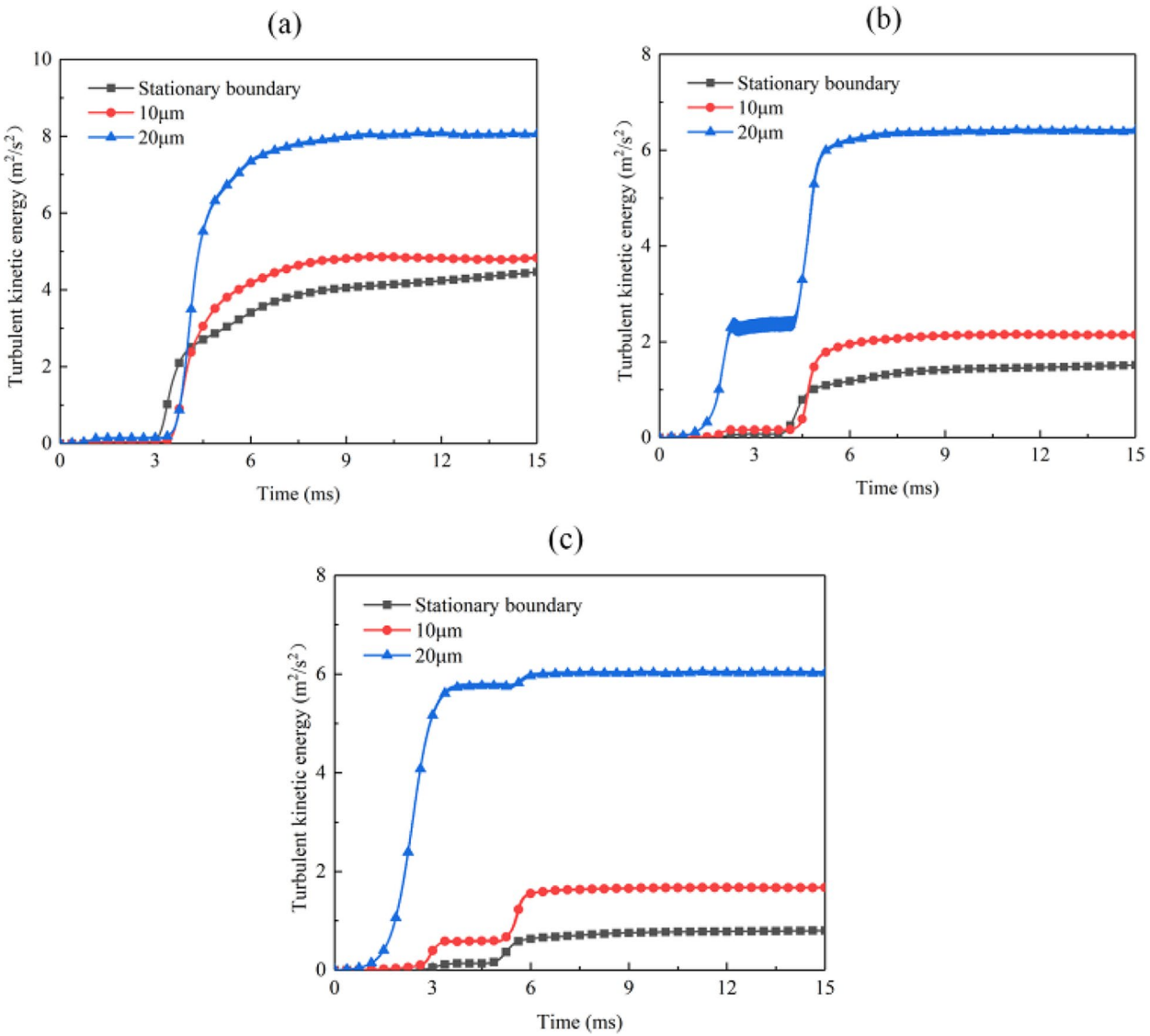

Figure 8 Turbulent kinetic energy time-varied waves: (**a**) $x = 40$ mm, (**b**) $x = 70$ mm, (**c**) $x = 100$ mm

flow from the turbulence generator is more pronounced when the monitoring point is closer to the turbulence generator.

The turbulent kinetic energy in the constrained flow channel is also related to the ultrasonic amplitude. The time-varied waves of the three monitoring points are obtained, as shown in Figure 8, where the ultrasound frequency is 40 kHz. The trend of the turbulent kinetic energy at different ultrasound amplitudes is the same. If the ultrasound amplitude rise, the turbulent kinetic energy curve becomes steeper. It indicates that the rate of the turbulent kinetic energy change is faster at higher ultrasound amplitude.

In order to study further the relationship between ultrasonic vibration and flow field, the detection line near the work-piece surface is selected, as shown in Figure 2(3). Then the turbulent kinetic energy waves of the stable states along the detection line about different ultrasonic frequencies are extracted, as is shown in Figure 9. With the increase of x coordinate, the energy dissipation caused by the viscous resistance of the flow channel wall reduces the turbulent kinetic energy of the flow field. In the absence of ultrasonic vibration, the turbulent kinetic energy decreases rapidly. Especially in the latter half of the constrained flow channel, the turbulent kinetic energy tends to be zero. This phenomenon of energy dissipation not only reduces the machining efficiency of the

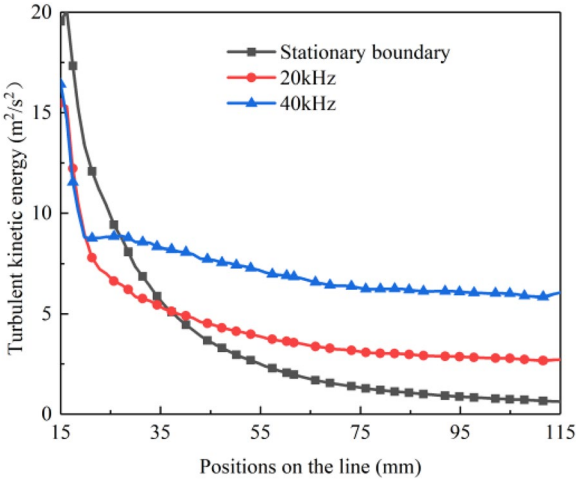

Figure 9 Turbulent kinetic energy waves for different ultrasonic frequencies

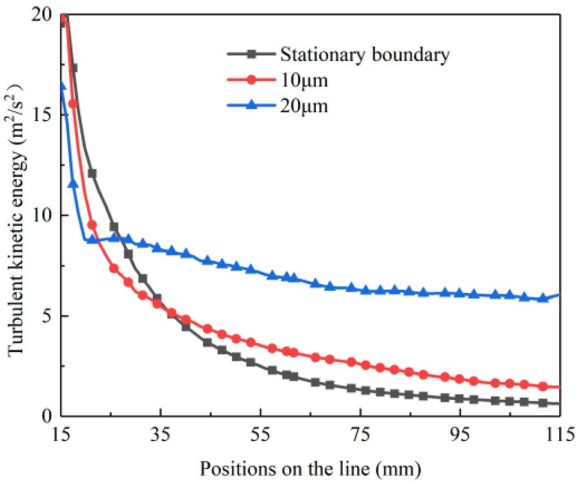

Figure 10 Turbulent kinetic energy waves for different ultrasonic amplitudes

SAF method, but also affects the uniformity of the work-piece surface. By comparing the three simulation curves, it can be inferred that the turbulent kinetic energy of the whole flow channel is enhanced after loading ultrasonic vibration. The turbulent kinetic energy of the flow channel loaded with 40 kHz ultrasonic vibration is twice that of the flow channel loaded with 20 kHz, and the curve of 40 kHz ultrasonic vibration has the best uniformity. So the machining efficiency and uniformity depend on the ultrasonic frequency, and they have a positive correlation.

Figure 10 shows the cases with different amplitudes, and the frequency is 40 kHz. The curve of turbulent kinetic energy is similar to Figure 9, and it shows a downward trend. Figure 10 shows that increasing the amplitude of ultrasonic vibration can also increase the turbulent kinetic energy. The effect of the ultrasonic wave with an amplitude of 20 μm on the turbulent kinetic energy is much more significant than that of 10 μm.

The above phenomenon is with a significant reference value for the ultrasonic assisted SAF processing technologies, that is, the ultrasonic vibration method might improve the machining efficiency of the SAF method.

4 Polishing Experiments and Result Discussion

4.1 Experimental Setup

In order to verify the correctness and effectiveness of the flow field strengthening method in this paper, it is necessary to carry out the machining experiment[53]. For the issue, an ultrasonic assisted machining device for the SAF method is built in this paper, as shown in Figure 11. The ultrasonic vibrator transmits the ultrasonic vibration to the constrained flow channel through the constraint module, and the soft abrasive flow in the flow channel will polish the test sample.

In this paper, two rectangular metal test samples with the same material and roughness are selected for comparison. One of them is processed by SAF processing without ultrasonic excitation, while the other one is processed by ultrasonic assisted SAF processing. The test samples are 100 mm long, 10 mm wide, 5 mm high, and the initial surface roughness is 1 μm.

Figure 11(6) shows the position of measuring points on the work-piece surface, there are nine measuring points and they are located at the entrance, middle, and exit of the work-piece surface. The surface roughness of each region is the average roughness of the three points in the corresponding region. In this paper, the processing experiment is carried out for 24 h, and the samples are measured every two hours.

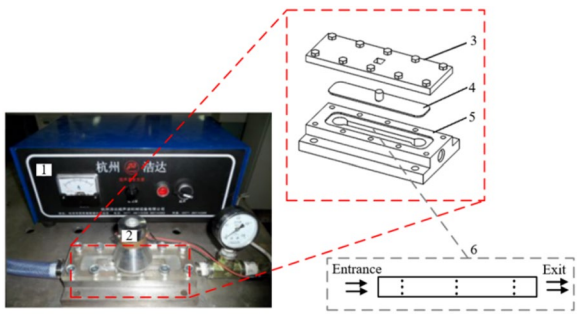

Figure 11 The ultrasonic assisted machining device: 1. Ultrasonic transducer, 2. Ultrasonic vibrator, 3. Cover plate, 4. Constraint module, 5. Base and constraint flow channel, 6. Test sample

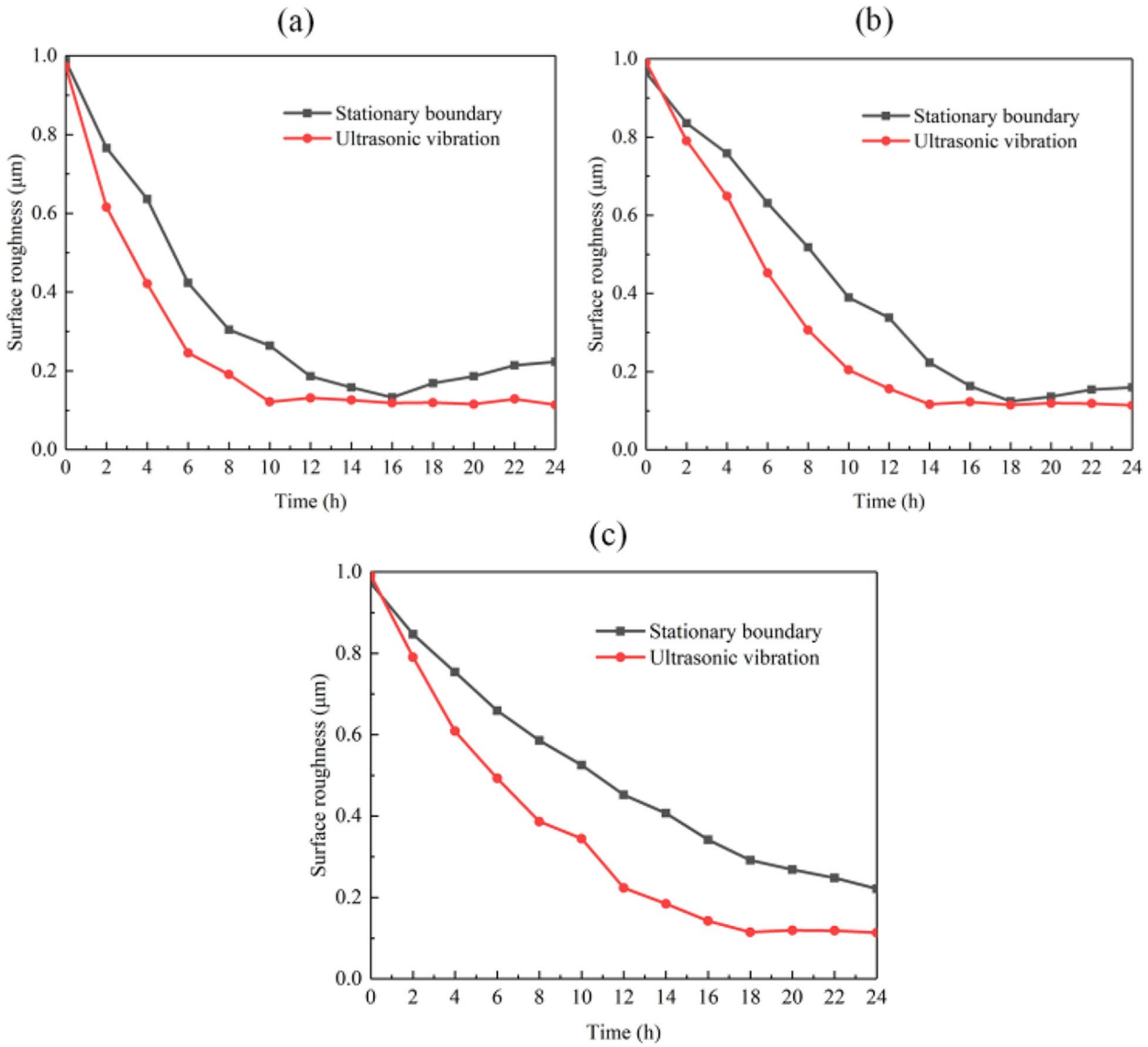

Figure 12 Surface roughness time-varied waves for different regions: (**a**) Entrance, (**b**) Middle, (**c**) Exit

4.2 Polishing Results and Discussion

It is well that surface roughness is a necessary physical parameter to characterize the polishing effect. Therefore, the surface roughness time-varied waves of the three regions are acquired, as shown in Figure 12.

From Figure 12(a), the following regulars can be acquired. It takes about 16 h for the surface roughness to reach 0.1 μm at the entrance of the sample without the ultrasonic vibration, and then the surface roughness increase slightly. The motion track of abrasive particles is single due to the weak turbulent kinetic energy, so the surface roughness is increased by micro-cutting in a single direction. However, it only takes about 10 h for the surface roughness to reach 0.1 μm with ultrasonic vibration, and the surface roughness remains constant after reaching the minimum value. The result indicates that ultrasonic cavitation enhances the turbulence intensity and makes the motion track of the abrasive particles complex and changeable, thus avoiding continuous cutting in a single direction.

From Figure 12(b), the regulars in the middle of the sample can be described. The surface roughness of the sample with the ultrasonic vibration reaches the minimum value about 4 h earlier than that without ultrasonic vibration. The material removal efficiency is significantly improved, and the stability of the SAF processing is maintained. Figure 12(c) shows the variation of the turbulent kinetic energy of the sample exit. After 18 h

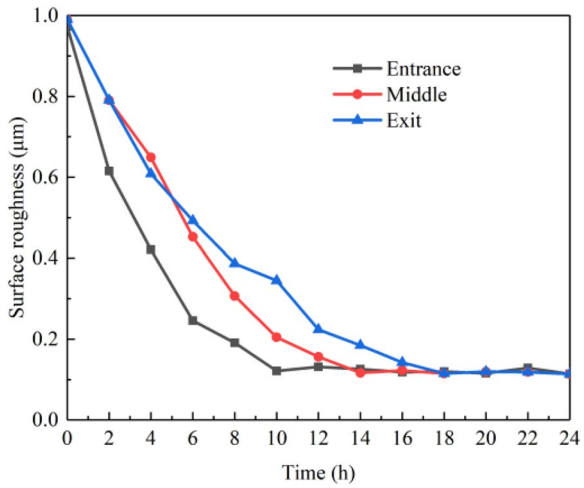

Figure 13 Surface roughness time-varied waves

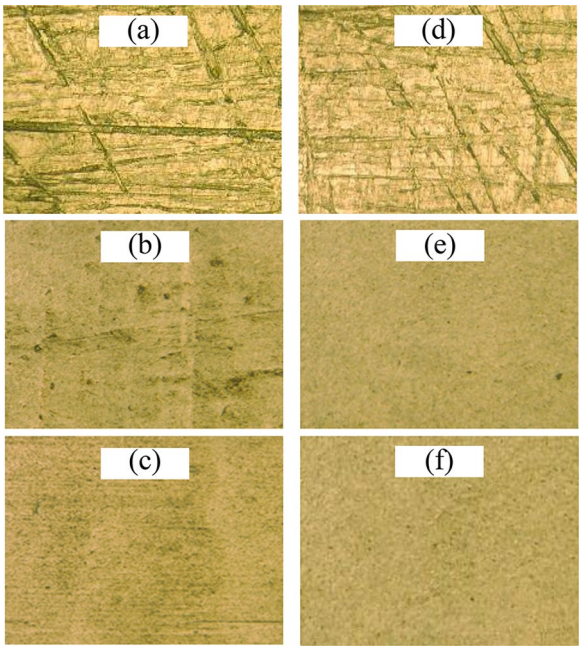

Figure 14 Surface topographies of the sample inlets: (**a**) $t = 0$ h, (**b**) $t = 8$ h, (**c**) $t = 24$ h, (**d**) $t = 0$ h, (**e**) $t = 8$ h, (**f**) $t = 24$ h

of processing, the surface roughness of the sample with ultrasonic vibration remains at about 0.1 μm, and the processing effect of ultrasonic vibration is still better than that without ultrasonic vibration.

The above results fully prove that the surface roughness of the sample with ultrasonic vibration decreases significantly faster at any position, and the polishing efficiency of the SAF method is improved by loading ultrasonic vibration.

Subsequently, to analyze the overall uniformity of the ultrasonic assisted SAF processing method, the surface roughness time-varied waves of each region are shown in Figure 13. As can be seen from the figure, the decrease rate of the surface roughness at the entrance is significantly faster than that at the other two positions, because the turbulence intensity is the strongest at the entrance. Moreover, in combination with the results in Figure 12, it can be inferred that although the surface roughness of the exit decreases at the slowest rate, the ultrasonic vibration can increase the processing efficiency appropriately.

Figure 14(a–c) shows the surface topographies of the sample inlets without ultrasonic vibration magnified by 500 times, and Figure 14(d–f) shows the surface topographies with ultrasonic vibration. As shown in the figure, the sample surfaces become more smooth after 8 h of processing. By comparing Figure 14(b) with Figure 14(e), it is evident that the ultrasonic assisted SAF method presents a better processing effect.

After 24 h of processing, some surface textures parallel to the flow direction of the soft abrasive flow appear on the sample's surface in Figure 14(c), which is consistent with the increase of the surface roughness in the later stage in Figure 12(a). The above situation is not apparent in Figure 14(f), which indicates that ultrasonic vibration can effectively inhibit the secondary processing of the sample by abrasive particles, and the uneven machining effect of the sample surface caused by the uneven distribution of turbulent kinetic energy can be improved.

5 Conclusions

The soft abrasive flow (SAF) machining method is an effective method for various structured surfaces, but its processing efficiency is low. In view of the shortcomings of the current SAF machining method, this paper presents the ultrasonic assisted SAF method. The corresponding research works have been performed, and the main conclusions are as follows.

(1) An acoustics-fluid coupling mechanic model is set up based on the realizable k-ε model and Helmholtz equation. Combined with the velocity profiles of the flow fields, it can be found that ultrasonic vibration can excite the cavitation effect in the flow field.
(2) The result of the simulation analysis shows the amplitude and frequency of ultrasonic vibration are the key factors affecting the turbulent kinetic energy in the flow field. With the increment of ultrasonic frequency and amplitude, the turbulence intensity of the flow field increases. The turbulent kinetic energy of the flow channel loaded with 40 kHz ultrasonic vibration is twice that of the flow

channel loaded with 20 kHz, and the curve of 40 kHz ultrasonic vibration has the best uniformity.

(3) A set of comparative polishing experiments with or without ultrasonic vibration are conducted to explore the performance of the ultrasonic assisted method. At the late stage of the SAF polishing, the abrasive particles continuously cut the work-piece surface in a single direction, which improves the surface roughness of the work-piece. The above problem can be improved obviously by ultrasonic vibration. The experiments show that ultrasonic vibration can improve the processing efficiency and uniformity of the SAF method.

Acknowledgements
Not applicable.

Author Contributions
TD was in charge of the whole trial; NY wrote the manuscript; TY assisted with sampling and laboratory analyses. All authors read and approved the final manuscript.

Authors' Information
Yesha Ni, born in 1992, is currently a PhD candidate at *College of Mechanical Engineering, Zhejiang University of Technology, China*. His research interest is intelligent manufacturing.
Yunfeng Tan, born in 1991, is currently a PhD candidate at *College of Mechanical Engineering, Zhejiang University of Technology, China*. His main research interests include precision/ultra-precision machining technology.
Dapeng Tan, born in 1980, is currently a professor at *College of Mechanical Engineering, Zhejiang University of Technology, China*. His research interests are digital manufacturing and intelligent manufacturing.

Funding
Supported by National Natural Science Foundation of China (Grant No. 52175124), Zhejiang Provincial Natural Science Foundation (Grant No. LZ21E050003), and Fundamental Research Funds for the Zhejiang Universities (Grant No. RF-C2020004).

Declarations

Competing Interests
The authors declare no competing financial interests.

Received: 17 July 2022 Revised: 13 June 2023 Accepted: 15 June 2023
Published online: 30 June 2023

References

[1] X C Wang, C C Wang, C Y Wang, et al. Approach for polishing diamond coated complicated cutting tool: Abrasive flow machining (AFM). *Chinese Journal of Mechanical Engineering*, 2018, 31: 97.
[2] Z J Duan, C H Li, W F Ding, et al. Milling force model for aviation aluminum alloy: Academic insight and perspective analysis. *Chinese Journal of Mechanical Engineering*, 2021, 34: 18.
[3] Y Q Geng, Y Z Wang, J X Cai, et al. Fabrication of ordered micro/nano-structures using probe-based force-controlled micromachining system. *Chinese Journal of Mechanical Engineering*, 2022, 35: 139.
[4] Y Y Wang, Y L Zhang, D P Tan, et al. Key technologies and development trends in advanced intelligent sawing equipments. *Chinese Journal of Mechanical Engineering*, 2021, 34: 30.
[5] M Yang, C H Li, Y B Zhang, et al. Maximum undeformed equivalent chip thickness for ductile-brittle transition of zirconia ceramics under different lubrication conditions. *International Journal of Machine Tools and Manufacture*, 2017, 122: 55-65.
[6] T Wang, C Y Wang, Y X Yin, et al. Analytical approach for nonlinear vibration response of the thin cylindrical shell with a straight crack. *Nonlinear Dynamics*, 2023, DOI: https://doi.org/10.1007/s11071-023-08460-4.
[7] J X Wang, S B Gao, Z J Tang, et al. A context-aware recommendation system for improving manufacturing process modeling. *Journal of Intelligent Manufacturing*, 2023, 34(3): 1347-1368.
[8] Y B Zhang, C H Li, H J Ji, et al. Analysis of grinding mechanics and improved predictive force model based on material-removal and plastic-stacking mechanisms. *International Journal of Machine Tools and Manufacture*, 2017, 122: 81-97.
[9] J Q Ge, S M Ji, D P Tan. A gas-liquid-solid three-phase abrasive flow processing method based on bubble collapsing. *International Journal of Advanced Manufacturing Technology*, 2018, 95: 1069-1085.
[10] X Zeng, S M Ji, M S Jin, et al. Investigation on machining characteristic of pneumatic wheel based on softness consolidation abrasives. *International Journal of Precision Engineering and Manufacturing*, 2014, 15(10): 2031–2039.
[11] S M Ji, Y W Chi, D P Tan, et al. Flow field characteristics of soft abrasive flow in multiform restraint flow passages. *Transactions of the Chinese Society of Agricultural Engineering*, 2011, 27(11): 71-77.
[12] S M Ji, J Q Zhong, D P Tan, et al. Research of distribution and dynamic characteristic of particle group in the structural flow passage. *Key Engineering Materials*, 2012, 499: 271-276.
[13] S M Ji, X X Weng, D P Tan. Analytical method of softness abrasive two-phase flow field based on 2D model of LSM. *Acta Physica Sinica*, 2012, 61(1): 31-37.
[14] D P Tan, S M Ji, Y Z Fu, An improved soft abrasive flow finishing method based on fluid collision theory. *Int J Adv Manuf Technol*, 2016, 85: 1261-1274.
[15] S M Ji, J Q Ge, D P Tan, et al. Three-phase abrasive flow polishing and distribution characteristics of bubble collapse. *Optics and Precision Engineering*, 2018, 26(2): 388-398.
[16] L Zhang, Z M Yuan, D P Tan, et al. An improved abrasive flow processing method for complex geometric surfaces of Titanium alloy artificial joints. *Applied Sciences*, 2018, 8(7): 1037.
[17] L Zhang, Z M Yuan, Z J Qi, et al. CFD-based study of the abrasive flow characteristics within constrained flow passage in polishing of complex titanium alloy surfaces. *Powder Technology*, 2018, 333: 209-218.
[18] C Li, Q D Xu, J Q Ge, et al. Study of soft abrasive flow field measurement based on particle image velocimetry. *The International Journal of Advanced Manufacturing Technology*, 2020, 109: 2039-2047.
[19] C Li, Q D Xu, J Q Ge, et al. Research on the incidence of soft abrasive flow to a wall and the machining characteristics. *The International Journal of Advanced Manufacturing Technology*, 2020, DOI: https://doi.org/10.1177/0954405420937559.
[20] J Q Ge, Y L Ren, X S Xu, et al. Numerical and experimental study on the ultrasonic-assisted soft abrasive flow polishing characteristics. *The International Journal of Advanced Manufacturing Technology*, 2021, 112: 3215-3233.
[21] M Ge, S M Ji, D P Tan. Erosion analysis and experimental research of gas-liquid-solid soft abrasive flow polishing based on cavitation effects. *International Journal of Advanced Manufacturing Technology*, 2021, 114: 3419-3436.
[22] J Q Ge, W P Hu, Y X Xi, et al. Gas-liquid-solid swirling flow polishing and bubble collapse impact characsteristics. *Powder Technol*, 2021, 390: 315-329.
[23] J Q Ge, H T Zhou, C Li, et al. Soft abrasive flow polishing method and optimization research on the constrained space. *International Journal of Advanced Manufacturing Technology*, 2022, 118: 1673-1688.
[24] Y F Tan, Y S Ni, J F Wu, et al. Machinability evolution of gas-liquid-solid three-phase rotary abrasive flow finishing. *The International Journal of Advanced Manufacturing Technology*, 2023, DOI: https://doi.org/10.1007/s00170-022-10761-8.
[25] J Q Ge, C Li, Z Y Gao. Softness abrasive flow polishing method using constrained boundary vibration. *Powder Technology*, 2021, 382: 173-187.

[26] Y Y Yang, M Yang, C H Li, et al. Machinability of ultrasonic vibration assisted micro-grinding in biological bone using nanolubricant. *Frontiers of Mechanical Engineering*, 2023, 18(1): 1.
[27] D Z Jia, C H Li, Y B Zhang, et al. Experimental evaluation of surface topographies of NMQL grinding ZrO2 ceramics combining multiangle ultrasonic vibration. *The International Journal of Advanced Manufacturing Technology*, 2019, 100: 457-473.
[28] J Q Ge, Y L Ren, C Li, et al. Ultrasonic coupled abrasive jet polishing (UC-AJP) of glass-based micro-channel for micro-fluidic chip. *International Journal of Mechanical Sciences*, 2023, 244(15): 108055.
[29] L Li, Y F Tan, Y S Ni, et al. Fluid-induced transport dynamics and vibration patterns of multiphase vortex in the critical transition states. *International Journal of Mechanical Sciences*, 2023, 252: 108376.
[30] L Li, Y S Yang, W X Xu, et al. Advances in the multiphase vortex-induced vibration detection method and its vital technology for sustainable industrial production. *Applied Sciences*, 2022, 12(17): 8538.
[31] D P Tan, Y S Ni, L B Zhang. Two-phase sink vortex suction mechanism and penetration dynamic characteristics in ladle teeming process. *Journal of Iron and Steel Research International*, 2017, 24(7): 669-677.
[32] L Li, W X Xu, Y F Tan, et al. Fluid-induced vibration evolution mechanism of multiphase free sink vortex and the multi-source vibration sensing method. *Mech Syst Signal Process*, 2023, 189: 110058.
[33] Z C Yin, Y S Ni, L Li, et al. Numerical modelling and experimental investigation of a two-phase sink vortex and its fluid-solid vibration characteristics. *Journal of Zhejiang University-SCIENCE A*, 2022, DOI: https://doi.org/10.1631/jzus.A2200014.
[34] T Wang, L Li, Z C Yin, et al. Investigation on the flow field regulation characteristics of the right-angled channel by impinging disturbance method. *Proceedings of the Institution of Mechanical Engineers Part C-Journal of Mechanical Engineering Science*, 2022, 236(23): 11196-11210.
[35] Y Huang, J Li, J C Yang, et al. Simulation Analysis of Torsion Beam Hydroforming Based on the Fluid-Solid Coupling Method. *Chinese Journal of Mechanical Engineering*, 2023, 36: 3.
[36] J Q Ge, H T Zhou, C Li, et al. Soft abrasive flow polishing method and optimization research on the constrained space. *International Journal of Advanced Manufacturing Technology*, 2021, 118(5-6): 1673-1688.
[37] L Li, D P Tan, Z C Yin, et al. Investigation on the multiphase vortex and its fluid-solid vibration characters for sustainability production. *Renewable Energy*, 2021, 175: 887-909.
[38] G A Zheng, Z H Gu, W X Xu, et al. Gravitational surface vortex formation and suppression control: A review from hydrodynamic characteristics. *Processes*, 2023, 11(1): 42.
[39] L Li, B Lu, W X Xu, et al. Mechanism of multiphase coupling transport evolution of free sink vortex. *Acta Phys. Sin.*, 2023, 72(3): 034702.
[40] L Li, Z H Gu, W X Xu, et al. Mixing mass transfer mechanism and dynamic control of gas-liquid-solid multiphase flow based on VOF-DEM coupling. *Energy*, 2023, 272: 127015.
[41] M D Li, D C Kong, Q Guo, et al. Investigation of movement and deposition behaviors of solid particles in hydraulic water reservoir via the CFD-DEM coupling method. *Chinese Journal of Mechanical Engineering*, 2022, 35:118.
[42] L Li, D P Tan, T Wang, et al. Multiphase coupling mechanism of free surface vortex and the vibration-based sensing method. *Energy*, 2021, 216: 119136.
[43] X H Fan, D P Tan, L Li, et al. Modeling and solution method of gas-liquid-solid three-phase flow mixing. *Acta Physica Sinica*, 2021, 70: 124501.
[44] G A Zheng, J L Shi, L Li, et al. Fluid-solid coupling-based vibration generation mechanism of the multiphase vortex. *Processes*, 2023, 11(2): 568.
[45] S H Zheng, Y K Yu, M Z Qiu, et al. A modal analysis of vibration response of a cracked fluid-filled cylindrical shell. *Applied Mathematical Modelling*, 2021, 91: 934-958.
[46] Y Pan, S M Ji, D P Tan. Cavitation based soft abrasive flow processing method. *International Journal of Advanced Manufacturing Technology*, 2020, 109(9): 2587-2602.
[47] F Z Li, H Y Fan, Y Q Guo, et al. Water-Jet Cavitation Shock Bulging as Novel Microforming Technique. *Chinese Journal of Mechanical Engineering*, 2021, 34: 4.
[48] D H Wu, Y Ren, Y Q Gu, et al. Unsteady Flow and Structural Behaviors of Centrifugal Pump under Cavitation Conditions. *Chinese Journal of Mechanical Engineering*, 2019, 32: 17.
[49] Y H Gu, G A Zheng. Dynamic Evolution Characteristics of the Gear Meshing Lubrication for Vehicle Transmission System. *Processes*, 2023, 11(2): 561.
[50] S T Chen, D P Tan. A SA-ANN-based modeling method for human cognition mechanism and the PSACO cognition algorithm. *Complexity*, 2018: 6264124.
[51] D P Tan, S T Chen, G J Bao, et al. An embedded lightweight GUI component library and the ergonomics optimization method for industry process monitoring. *Frontiers of Information Technology & Electronic Engineering*, 2018, 19(5): 604-625.
[52] H P Lyu, L B Zhang, D P Tan, et al. A collaborative assembly for low-voltage electrical apparatuses. *Frontiers of Information Technology & Electronic Engineering*, 2022, DOI: https://doi.org/10.1631/FITEE.2100423.
[53] X T Wei, C X Yue, D S Hu, et al. Research on Surface Roughness of Supersonic Vibration Auxiliary Side Milling for Titanium Alloy. *Chinese Journal of Mechanical Engineering*, 2022, 35: 10.

Submit your manuscript to a SpringerOpen journal and benefit from:

► Convenient online submission
► Rigorous peer review
► Open access: articles freely available online
► High visibility within the field
► Retaining the copyright to your article

Submit your next manuscript at ► springeropen.com